Volume 2
Number 6
November 2024
Pages 1179–1322

EES Catalysis

rsc.li/EESCatalysis

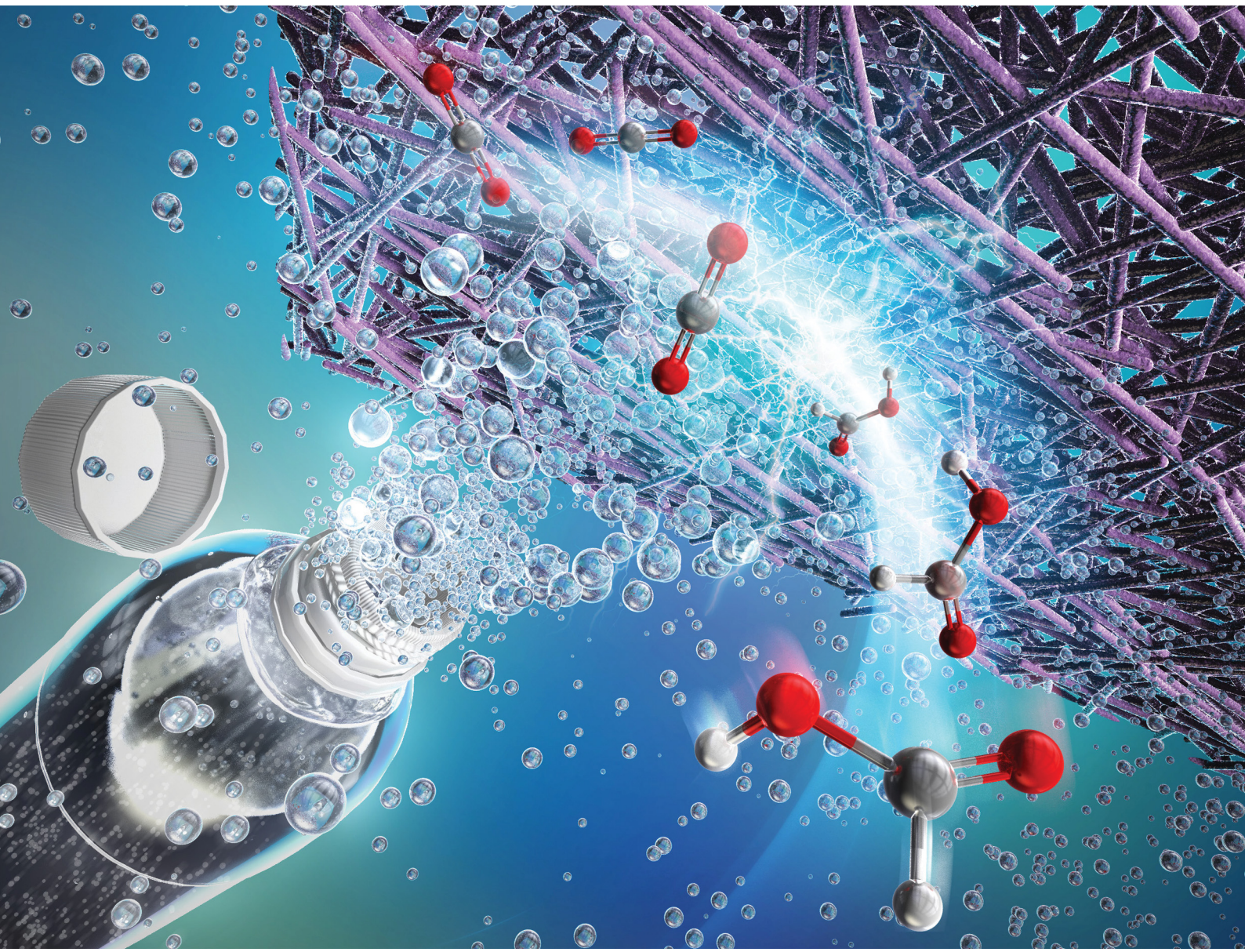

ISSN 2753-801X

ROYAL SOCIETY OF CHEMISTRY

PAPER
Fumiaki Amano *et al.*
Highly selective formate formation *via* bicarbonate conversions

EES Catalysis

PAPER

View Article Online
View Journal | View Issue

Cite this: *EES Catal.*, 2024, 2, 1277

Highly selective formate formation *via* bicarbonate conversions†

Kohta Nomoto, Takuya Okazaki, Kosuke Beppu, Tetsuya Shishido and Fumiaki Amano *

Received 8th June 2024,
Accepted 19th August 2024

DOI: 10.1039/d4ey00122b

rsc.li/eescatalysis

Electrocatalytic conversion of liquid bicarbonate feedstock to formate is a promising reactive CO_2 capture technology. However, bicarbonate-fed electrolyzers have shown insufficient faradaic efficiencies (FEs) for formate production due to competing hydrogen evolution reactions. In this study, we developed a bicarbonate electrolyzer incorporating a porous membrane between a proton exchange membrane (PEM) and a hydrophilic bismuth cathode. By employing the intermediate membrane to enhance *in situ* CO_2 generation from 3.0 M $KHCO_3$, we achieved a formate FE of 84.6% even at a high current density of 300 mA cm^{-2}. This electrolyzer also achieved high CO_2 utilization efficiency (89%) and low full-cell voltage (3.1 V) at 100 mA cm^{-2} owing to the rational designs of membrane electrode assemblies. Bicarbonate conversion to formate is accelerated through *in situ* CO_2 generation and selective CO_2 reduction reaction at a gas–liquid–catalyst triple-phase boundary. Additionally, the bicarbonate electrolyzer demonstrates high CO_2 utilization efficiency, long-term stability, and production of pure formate salt.

Broader context

Carbon capture and utilization to convert atmospheric CO_2 into useful chemicals and fuels is essential for achieving a carbon-neutral or negative emission future. Electrochemical CO_2 reduction reaction (CO_2RR) can directly produce formate, carbon monoxide, ethylene, and other compounds using renewable energy at room temperature and pressure. However, significant energy is lost in supplying high-purity CO_2 to conventional CO_2RR reactors with a gas-diffusion electrode, which also suffers from low carbon utilization efficiency. Reactive carbon capture, which converts CO_2 dissolved in alkaline solutions, addresses these challenges. We report a liquid bicarbonate-fed electrolyzer for formate production with a high selectivity (faradaic efficiency) of 85% at a high rate (current density) of 300 mA cm^{-2}. This highly selective formate production utilizes electrocatalytically inactive bicarbonate (hydrogen carbonate), avoiding the energy-intensive CO_2 separation and purification processes and enhancing carbon utilization efficiency. Formate, the smallest carboxylate, is expected to serve as an energy carrier for direct formate fuel cells. Thus, this bicarbonate electrolyzer contributes to realizing a decarbonized society through green transformation.

Introduction

The development of CO_2 recycling technology is crucial for achieving carbon neutrality. The electrocatalytic CO_2 reduction reaction (CO_2RR) is promising for producing value-added chemicals efficiently at ambient temperature and pressure.[1,2] Among CO_2RR products, formic acid (HCOOH) and/or formate ($HCOO^-$) are valuable as energy carriers for fuel cells.[3–5] Electrocatalysts based on Bi, Sn, Hg, Pb, and In are predominantly used for formate formation due to their high selectivity.[2]

Recently, gas-fed CO_2 electrolyzers, where gaseous CO_2 is directly supplied, have attracted significant attention.[6–9] Gas diffusion electrodes (GDEs) enable the direct feeding of gaseous CO_2 to the electrocatalyst, mitigating CO_2 diffusion limitations. This allows for CO_2 electrolysis with higher current density and selectivity compared to CO_2 supply through bubbling into electrolyte solutions. However, GDE-based electrolyzers face challenges including carbon losses due to low single-pass conversion and CO_2 dissolution into alkaline electrolytes, and low stability due to GDE flooding and salt deposition.[10–12] Additionally, substantial energy is required to separate and compress pure CO_2 gas.[13] To address energy losses associated with carbon capture for gas-fed electrolyzers, reactive CO_2 capture (RCC) technology, which is defined as a direct chemical conversion of captured CO_2 into products, is gaining attention.[14,15] Electrochemically-driven RCC, by supplying aqueous solutions of bicarbonate (HCO_3^-) or carbonate (CO_3^{2-}), have been reported to convert *in situ* generated CO_2 in the (bi)carbonate electrolyzers.[15–23]

Department of Applied Chemistry for Environment, Tokyo Metropolitan University, 1-1 Minami-Osawa, Hachioji, Tokyo 192-0397, Japan. E-mail: f.amano@tmu.ac.jp

† Electronic supplementary information (ESI) available. See DOI: https://doi.org/10.1039/d4ey00122b

In the bicarbonate electrolyzer, HCO_3^- reacts with a proton near the polymer electrolyte membrane to produce CO_2 ($HCO_3^- + H^+ \rightarrow CO_2 + H_2O$, eqn (1)). The generated CO_2 gas is then electrocatalytically reduced to formic acid on the electrocatalyst ($CO_2 + 2H^+ + 2e^- \rightarrow HCOOH$, −0.17 V *vs.* SHE, eqn (2)). The generated formic acid exists as formate in the near-neutral electrolyte. Previous reports have shown that the faradaic efficiency (FE) for formate production in the bicarbonate electrolyzers is less than 70%.[20–22] This insufficient FE compared to gas-fed CO_2 electrolyzers is attributed to the undesirable hydrogen evolution reaction (HER, $2H^+ + 2e^- \rightarrow H_2$, 0 V, eqn (3)).

To improve the formate FE, it is crucial to mitigate the competitive HER in the bicarbonate-fed system. However, it has been noted that bicarbonate serves as an H^+ donor, complicating the suppression of HER.[20] Thus, the primary factors responsible for selective formate synthesis remain unclear in bicarbonate electrolyzers. Additionally, the bicarbonate electrolyzers for formate production employed a bipolar membrane (BPM) as the polymer electrolyte membrane, resulting in high full cell voltages of approximately 4.0 V at a current density of 100 mA cm^{-2}.[20,21] Proton exchange membrane (PEM) would be a solid polymer electrolyte more suitable for bicarbonate electrolyzers.

In this study, we aimed to improve the formate FE by optimizing the cathode configuration for efficient *in situ* CO_2 generation from aqueous potassium hydrogen carbonate ($KHCO_3$). To prevent increased H^+ concentration at the cathode electrocatalyst due to contact with PEM, hydrophilic porous membranes were reportedly introduced as an intermediate layer.[16,22,24] Here, we further investigate the critical role of the porous membrane for formate formation within bicarbonate electrolyzers (Fig. 1). We employed different porous membranes between PEM and a bismuth (Bi) catalyst cathode. We hypothesized that the intermediate layer provides the reaction field for the *in situ* CO_2 generation, transported to the porous cathode to form gas–liquid–catalyst triple-phase boundary. Using a 3.0 M $KHCO_3$ aqueous solution as a feedstock, formate FEs exceeding 80% and 90% were achieved over a porous Bi cathode at current densities of 300 and 100 mA cm^{-2}, respectively. Furthermore, we achieved a decrease in full cell voltage by employing an iridium oxide (IrO_2) catalyst for oxygen evolution reaction (OER) with PEM instead of BPM previously adopted for bicarbonate electrolyzers.[20,21]

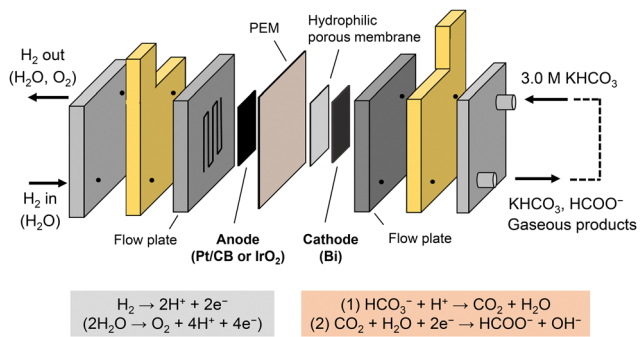

Fig. 1 Schematics of a bicarbonate-fed electrolyzer, wherein aqueous HCO_3^- reacts with H^+ near the proton exchange membrane (PEM) to produce CO_2 (eqn (1)), which is electrocatalytically reduced to formate on the Bi cathode (eqn (2)). A hydrophilic porous membrane between PEM and the cathode facilitates *in situ* CO_2 generation. Pt/CB or IrO_2 anodes are used for hydrogen oxidation and oxygen evolution reactions, respectively.

Results and discussion

Bicarbonate electrolyzer configuration

The Bi catalyst was electrochemically deposited on a carbon fibre paper at 8.0 mA cm^{-2} for 5 min (see details in the Experimental section). The catalyst loading amount was 1.7 mg cm^{-2} (28.5 wt%), and the FE of electrodeposition ($Bi^{3+} + 3e^- \rightarrow Bi$, eqn (4)) was nearly 100% based on the deposited catalyst weight. X-ray diffraction (XRD) analysis revealed that rhombohedral Bi crystals are deposited on the carbon paper (Fig. 2a). The crystalline size of Bi (012) was 43.3 nm, determined using Scherrer's equation. Raman spectroscopy detected E_g (71 cm^{-1}) and A_{1g} (98 cm^{-1}) bands of metallic Bi (Fig. 2b).[25] Scanning electron microscopy–energy dispersive X-ray spectroscopy (SEM–EDS) analysis confirmed the uniform deposition of Bi crystallites (particle size, approximately 5–10 μm) on carbon fibres (Fig. 2c).

Fig. 3 shows the results of electrocatalytic bicarbonate conversion at a current density of 100 mA cm^{-2}. First, a platinum-loaded carbon black (Pt/CB) catalyst under humidified H_2 flow was used as an anode for hydrogen oxidation reaction (HOR). The full cell voltage of the HOR|PEM|HCO_3^- configuration at low current density would be the half-cell potential relative to a reversible hydrogen electrode (RHE). An aqueous solution with

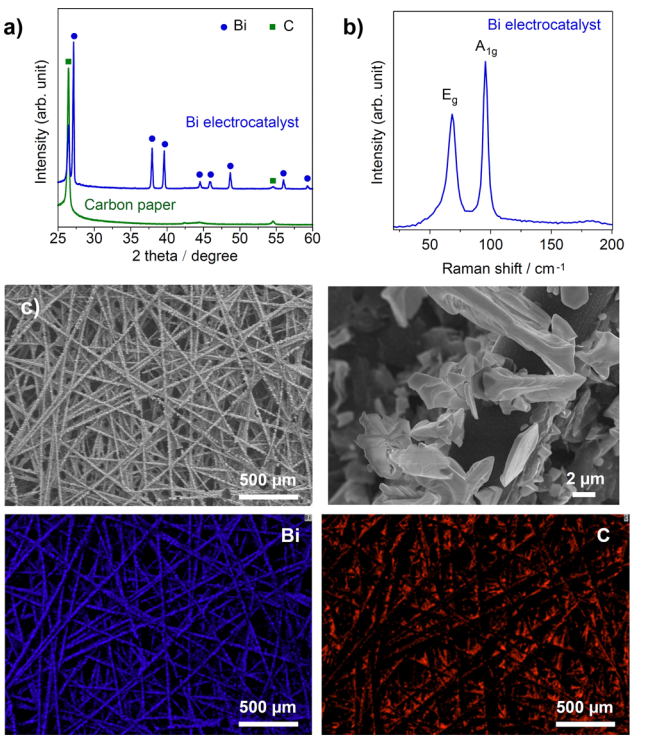

Fig. 2 (a) XRD pattern, (b) Raman spectrum, and (c) SEM images and EDS elemental mappings of Bi electrocatalyst deposited on carbon fibre paper.

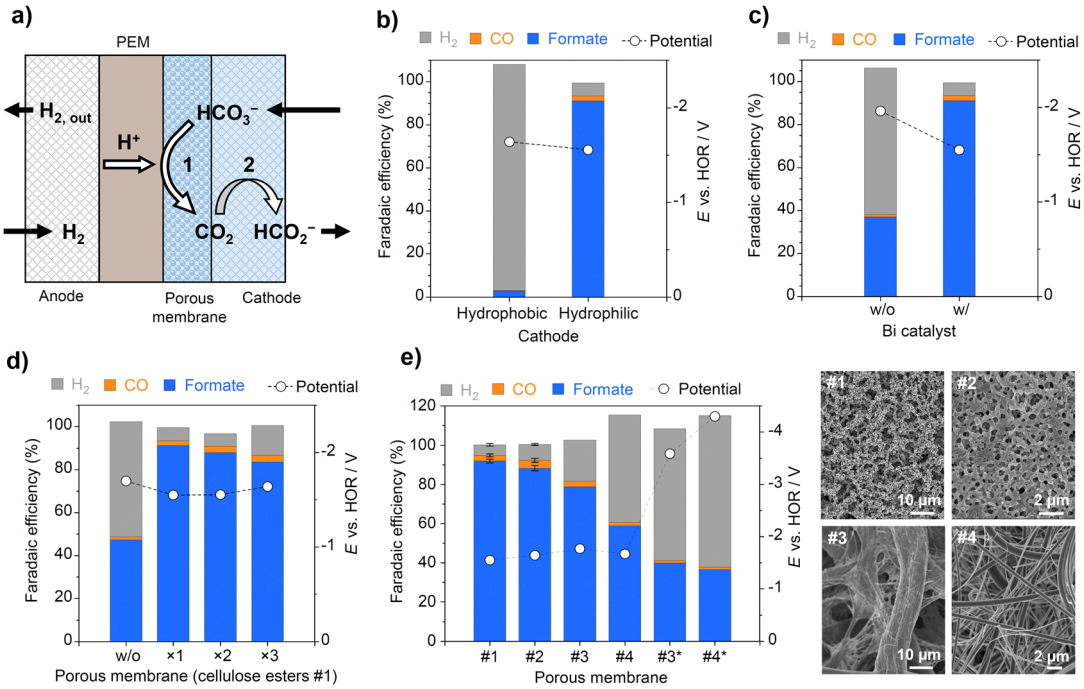

Fig. 3 (a) Schematic of bicarbonate electrolyzer with Pt/CB anode for HOR (HOR|PEM|HCO_3^-). FE of each product for (b) hydrophobic *versus* hydrophilic Bi cathodes and (c) with and without Bi catalyst in the hydrophilic cathode. The full-cell potential (*vs.* HOR) is shown on the right *y*-axis. (d) Effect of number of the intermediate porous membrane (#1, mixed cellulose esters, thickness 150 μm). (e) Effect of the type of intermediate porous membranes (see Table 1 for the details) and SEM images of membrane #1, #2, and #4. The membranes #3* and #4* were functionalized with an alkaline ionomer (Sustanion XA-9). Electrocatalytic reactions were performed at 100 mA cm^{-2} with 3.0 M $KHCO_3$ (pH 8.5) at a flow rate of 32 mL min^{-1}.

3.0 M $KHCO_3$ (pH 8.5) in open air was circulated by a peristaltic pump. The electrodeposited Bi catalyst served as the porous cathode for circulating 3.0 M $KHCO_3$ aqueous solution (Fig. 3a). Contact angle measurements confirmed the hydrophilicity of the Bi cathode (Fig. S1, ESI†). We used a mixed cellulose esters membrane (thickness 150 μm, pore size 8 μm, #1) as a porous layer interposed between PEM and the cathode, according to the report for a carbonate electrolyzer.[16] The intermediate layer affects the pH gradient by physically separating the cathode electrode from the PEM surface with low pH.

When employing a hydrophobic Bi cathode, the formate FE was only 3.0%, with H_2 being the main product at 100 mA cm^{-2} (Fig. 3b). The Bi cathode was functionalized with polytetrafluoroethylene (PTFE) particles and exhibited hydrophobic behaviour with a contact angle of 142° (Fig. S1, ESI†). In contrast, utilizing the hydrophilic Bi cathode increased the formate FE to 91.2%, with H_2 and CO FEs at 5.9% and 2.4%, respectively. Proton nuclear magnetic resonance (^{1}H NMR) analysis confirmed the absence of other byproducts in the electrolyte (Fig. S2, ESI†). In the absence of Bi catalyst on the carbon paper substrate, the formate FE was reduced to 37.0% with an increase in the overpotential at 100 mA cm^{-2}, highlighting the effect of electrocatalyst for enhanced CO_2 conversion activity and formate selectivity (Fig. 3c). The general rate-determining step in CO_2RR is the initial one-electron transfer to surface-adsorbed CO_2, followed by the receipt of H^+ to form the *OCHO intermediate with the oxygen atom binding to the catalytic site for formate production.[2,26,27]

The hydrophobic cathode likely hindered the transport of bicarbonate solution to interface between PEM and porous membrane, impeding the reaction of HCO_3^- with H^+ (eqn (1)), and thus limiting *in situ* CO_2 generation. Consequently, undesired HER occurred selectively due to inadequate CO_2 supply to the cathode catalyst. On the other hand, the hydrophilic cathode facilitates efficient transport of the bicarbonate solution to the PEM/porous layer interface, enabling effective neutralization of H^+ with HCO_3^-. This promoted *in situ* CO_2 generation from the bicarbonate solution, increasing the CO_2 volume ratio near the Bi catalyst and enhancing the formate FE. These findings underscore the suitability of a hydrophilic Bi cathode for efficient formate formation (FE over 90%) at 100 mA cm^{-2}.

In the absence of the intermediate porous membrane, H_2 FE increased, and the formate FE decreased to 47.3% (Fig. 3d). This decrease occurred because direct contact between the cathode and PEM increased the H^+ concentration on the Bi catalyst. The slight increase in electrode potential also suggests insufficient CO_2 supply to the cathode due to H^+ consumption from HER. In a carbonate electrolyzer for C_{2+} formation, thick intermediate layers dramatically decreased the C_{2+} FE due to reduced CO_2 concentration from reaction with carbonate ($CO_2 + CO_3^{2-} + H_2O \rightarrow 2HCO_3^-$, eqn (5)).[16] We found that the effect of the thickness (150–450 μm) on the formate FE was not significant in the case of bicarbonate electrolyzer, likely because CO_2 capture does not occur in 3.0 M $KHCO_3$. However, increasing the thickness slightly decreased the formate FE from 91.2% (×1, 150 μm) to 88.0% (×2, 300 μm) and 83.6% (×3, 450 μm). This suggests that the spacing

Table 1 Properties of intermediate porous membranes (#1–#4) used in Fig. 3e

Membrane	Material	Mass (mg cm^{-2})	Thickness (μm)	Porosity[b] (%)	Pore size[c] (μm)
#1	Mixed cellulose esters[a]	3.58	150	84	8
#2	Mixed cellulose esters[a]	3.77	110	77	0.2
#3	α-Cellulose	9.33	210	70	6
#4	Borosilicate glass	5.41	220	89	0.6

[a] Composed of nitrocellulose (~84%) and acetylcellulose with a small amount of polyoxyethylene octylphenyl ether. [b] Porosity calculated from the mass and thickness measurements, assuming that the densities of celluloses and borosilicate are 1.5 and 2.2 g cm^{-3}. [c] Pore size reported by suppliers.

with longer distances prevents smooth access of aqueous $KHCO_3$ near the PEM.

We then explored the intermediate porous layer with different material composition and properties (Table 1). SEM images of the porous membranes are shown in Fig. 3e and Fig. S3 (ESI†). For the mixed cellulose esters, the FE was slightly decreased with decreasing pore size from 91.2% (#1, 8 μm) to 87.3% (#2, 0.2 μm), but the influence of the pore size and morphology difference was not so significant (Fig. 3e). We did not find a strong relationship between physical properties (pore size, thickness, and porosity) and electrolyzer performance. In contrast, we found that the use of pristine α-cellulose (#3) and borosilicate glass fibres (#4) significantly decreased the formate FE, suggesting that the material composition significantly affects *in situ* CO_2 generation through the protonation of bicarbonate ions. Functionalization with an alkaline ionomer further decreased the formate FE and increased the overpotential probably due to the decreased proton conductivity. These results highlight the crucial role in creating not only a pH gradient space to decrease the H^+ concentration on the cathode but also a reaction field for neutralization of proton by bicarbonate. The chemical properties of cellulose esters impact *in situ* CO_2 generation on the surface in the porous structure with a large surface area. When focusing only on cellulose membranes, the formate FE gradually increases with the porosity, which is estimated from mass and thickness.

Bicarbonate flow conditions

To investigate the influence of the bicarbonate feedstock supply on the interface between PEM and porous membrane, two flow fields with different channel designs were employed for the cathode (Fig. 4a). Compared to a serpentine flow channel, a grid flow channel resulted in decreased H_2 FE and increased formate FE. The gaseous CO_2 evolution rate from the cell outlet, not consumed by CO_2RR, was 0.66 and 0.84 mmol h^{-1} for the serpentine and grid channels, respectively. The CO_2 utilization efficiency, calculated as the ratio of products to *in situ* generated CO_2, was 89% and 88% for the serpentine and grid channels, respectively, indicating no significant difference between them. This suggests that the enhanced formate FE with the grid channel is not attributed to an increased CO_2RR rate but rather to accelerated CO_2 generation near the PEM. The CO_2 utilization efficiency of over 89% indicates that most of the CO_2 generated inside the reactor was converted to formate. This CO_2 utilization efficiency greatly exceeds the value of existing gas-supplied electrolyzers (usually less than 10%) and surpasses that reported on the previous bicarbonate electrolyzer (~40%) for CO production.[28,29] The enhanced CO_2 utilization would be explained by the difference in the product form: CO is gas, but formate is liquid. When gaseous CO is the main product, *in situ* generated CO_2 is also released from the cathode with the bubbles of the gaseous products.

The flow rate dependence analysis of the bicarbonate solution revealed an increase in formate FE at higher flow rates for both flow channels (Fig. 4b and c). These findings suggest that a rapid supply of bicarbonate solution to the PEM efficiently suppresses HER and enhances CO_2 generation. Efficient delivery of HCO_3^- to the PEM interface by a grid flow channel facilitates H^+ consumption and promotes *in situ* CO_2 generation, resulting in HER suppression and improved formate FE. We found that reducing H^+ concentration at the cathode and efficient CO_2 generation by introducing an intermediate porous membrane contributes to enhanced formate FE (91% at 100 mA cm^{-2}). The grid flow channel and high flow rate of 3.0 M $KHCO_3$ also offer highly efficient formate production.

Performance of the bicarbonate reactor

The current density dependence was investigated under optimum reaction conditions (Fig. 5a). The formate FE was gradually increased with current density and maximized to 91.2% at 100 mA cm^{-2} and remained as high as 79.1% at 300 mA cm^{-2}. These formate FEs were much higher than those of previous bicarbonate electrolyzers, which achieved approximately 60% at 100 mA cm^{-2} and 40% at 300 mA cm^{-2}.[20,21] The formate FE decreased with increasing current density due to increased HER. Investigating the flow rate dependence at 300 mA cm^{-2} confirmed that the HER could be suppressed by further increasing the flow rate, reaching 84.6% FE at 64 mL min^{-1} (Fig. S4, ESI†). This suggests that at high current densities, the H^+ concentration at the cathode increases due to the increase in H^+ transport from the PEM. Therefore, a more efficient supply of bicarbonate is necessary to maintain high FEs at current densities above 100 mA cm^{-2}. At lower current densities, limited proton transport resulted in low FE due to insufficient CO_2 generation.

The electrocatalytic performance was also compared with a gas-fed CO_2 electrolyzer using the hydrophobic Bi cathode (Fig. 5b), with the configuration shown in Fig. S5 (ESI†). The FE and overpotential at 100 mA cm^{-2} were comparable to those of the state-of-the-art gas-fed CO_2 electrolyzer. This indicates that the CO_2RR electrocatalyst works well even in the liquid electrolyte, suggesting that the *in situ* generated CO_2 bubbles create gas–liquid–catalyst triple-phase boundaries in the porous Bi cathode. Linear sweep voltammetry (LSV) measurement in the gas-fed electrolyzer confirmed that HER

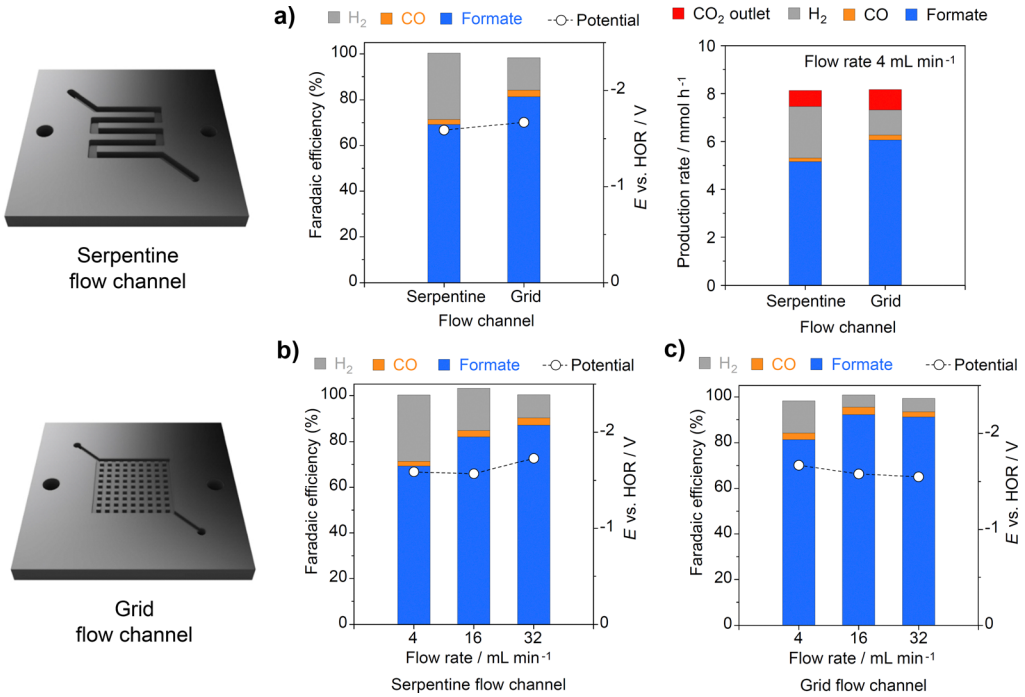

Fig. 4 (a) Influence of liquid flow channels on FEs of each product, full-cell potential (*vs.* HOR), production rate, and CO_2 outlet rate under 3.0 M $KHCO_3$ flow at 4 mL min^{-1}. Flow rate dependence on performances using flow field plates with (b) serpentine channel (width/depth: 2 mm) and (c) grid channel (width/depth: 1 mm). Electrocatalytic reactions were performed at 100 mA cm^{-2} with the intermediate cellulose esters membrane.

is promoted on the Bi cathode at potentials less than −1.5 V *vs.* RHE (Fig. S6, ESI†). Thus, developing CO_2RR electrocatalysts with high activity is crucial to decrease the overpotential at high current densities. In the absence of the Bi catalyst, the formate FE at 100 mA cm^{-2} in the gas-fed condition was only 8.1%, which is much lower than the 37.0% in the bicarbonate electrolyzer

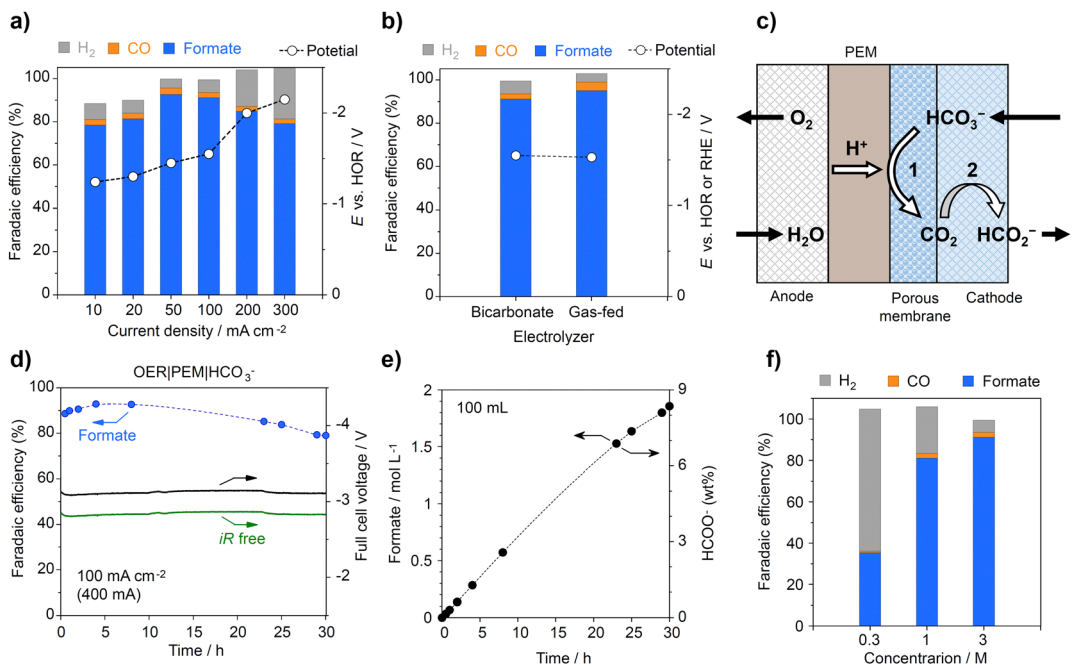

Fig. 5 (a) Effect of current density on product FEs and full-cell potential (*vs.* HOR). (b) Comparison between bicarbonate and gas-fed CO_2 electrolyzers at 100 mA cm^{-2}. (c) Schematics of bicarbonate electrolyzer using IrO_2 anode for OER (OER|PEM|HCO_3^-). (d) Time course of formate FE and full cell voltage (with and without *iR* compensation) in long-term stability test at 100 mA cm^{-2}. (e) Concentration of formate in the circulated 100 mL catholyte during the long-term test. (f) Effect of bicarbonate concentration on product FE. All reactions were performed with $KHCO_3$ flow at 32 mL min^{-1} using a grid flow plate.

without the Bi catalyst (Fig. 3c). It is noteworthy that the formate FE decreased to 1.1% when the flow channel plate was replaced from carbon to titanium, suggesting that the carbon plate may have contributed to the moderate FE without the Bi catalyst.

The bicarbonate-fed reaction was carried out for an extended period at 100 mA cm^{-2} using an IrO_2 anode as an OER catalyst (Fig. 5c). The formate FE remained above 90% initially and over 80% even after 30 hours. The full cell voltage was stable at 3.1 V (Fig. 5d), with a measured cell resistance of 2.64 Ω cm^2 (Fig. S7, ESI†), yielding an *iR*-free cell voltage of 2.8 V for the OER|PEM|HCO_3^- system. The full cell voltage is significantly lower than those reported for bicarbonate electrolyzers using BPM and Ni foam as the OER anode, ~4.0 V (without *iR* compensation).[20,21] We replaced BPM with PEM and used an IrO_2 anode suitable for acidic conditions, reducing the cell voltage required for water dissociation in BPM.[30,31]

In a conventional gas-fed CO_2 electrolyzer using an alkaline electrolyte, GDE performance reportedly declined over time due to flooding, where liquid penetrates hydrophobic GDE and blocks the gas diffusion path.[11,12] In contrast, this electrolyzer demonstrated long-term stability because the hydrophilic Bi cathode is operated under "flooding" conditions, avoiding the instability typical of GDE electrolyzers (flooding and salt deposition). Long-term stability is a key benefit of the bicarbonate electrolyzer using liquid feedstock to keep the gas–liquid–catalyst triple-phase boundary. It should be noted that instability was observed when using the Pt/CB anode; the overpotential gradually increased and current oscillations occurred in about 1–2 hours (Fig. S8, ESI†). This instability, which was not observed for the IrO_2 anode, is likely due to Pt catalyst poisoning by crossover CO generated at the cathode.[32]

The 30-h reaction at 100 mA cm^{-2} produced 1.9 M formate, equivalent to 8.6 wt% $HCOO^-$, in 100 mL electrolyte (Fig. 5e). The bicarbonate concentration was also steadily decreased over time (Fig. S9, ESI†). The formate yield was 63% (1.9 M $HCOO^-$ was converted from 3.0 M HCO_3^-, resulting in ~1.0 M HCO_3^-) for 100 mL catholyte. The formate FE was decreased at lower bicarbonate concentrations (Fig. 5f), suggesting that the gradual decrease in FE during the 30-h reaction was due to bicarbonate consumption.

Fig. 6 summarizes the performances of the bicarbonate electrolyzer compared to the previously reported values for formate formation.[20–22] The rational design of the membrane electrode assembly achieved a formate FE of 91.2% at 100 mA cm^{-2} and a full cell voltage of 3.1 V (Fig. 6a), contributing to energy savings in electrocatalytic reactions. Additionally, 84.6% formate FE was maintained at a high current density of 300 mA cm^{-2} (Fig. 6b). The partial current density for formate production, 254 mA cm^{-2}, is the highest among the electrolyzers using $KHCO_3$ feedstock.

In this bicarbonate-fed electrolyzer, unreacted HCO_3^- can be recycled by the liquid circulation, overcoming the main drawback of low carbon efficiency in gas-fed CO_2 electrolyzers (usually less than 10%). The bicarbonate electrolyzer also functions effectively in the presence of oxygen owing to the low solubility of O_2 in aqueous media.[33] These benefits are significant advantages of the bicarbonate-fed electrolyzer compared with gas-fed GDE systems.

We also confirmed the near-complete conversion of 50 mL of 3.0 M $KHCO_3$ to ~3.0 M formate (13.5 wt%) at 100 mA cm^{-2} (Fig. S10, ESI†). The bicarbonate feedstock was continuously bubbled with 100% CO_2 gas to make up the loss. The full cell voltage was constant during 44 h, suggesting that there is no salt precipitation and catalyst layer degradation. After the reaction, we collected the formate salts by evaporation to dryness and obtained 2.43 g of solid salt from the 10 mL catholyte. Powder XRD revealed the production of high-purity HCOOK crystallites without $KHCO_3$ contamination (Fig. 6c). The solid HCOOK could be an energy carrier suitable for long-term storage and long-distance transportation. Therefore, the highly selective formate synthesis sustained by bicarbonate feeding is a significant advance in the field of reactive CO_2 capture for energy conversion, storage, and transport. Future work will need to increase the geometrical electrode area (4.0 cm^2) to a typical lab device scale (25 cm^2).[34]

Experimental

To electrodeposit the bismuth catalyst, 0.8 g of $Bi(NO_3)_3$ $5H_2O$ (Fujifilm Wako Pure Chemical, 99.9%) was dissolved in 50 mL

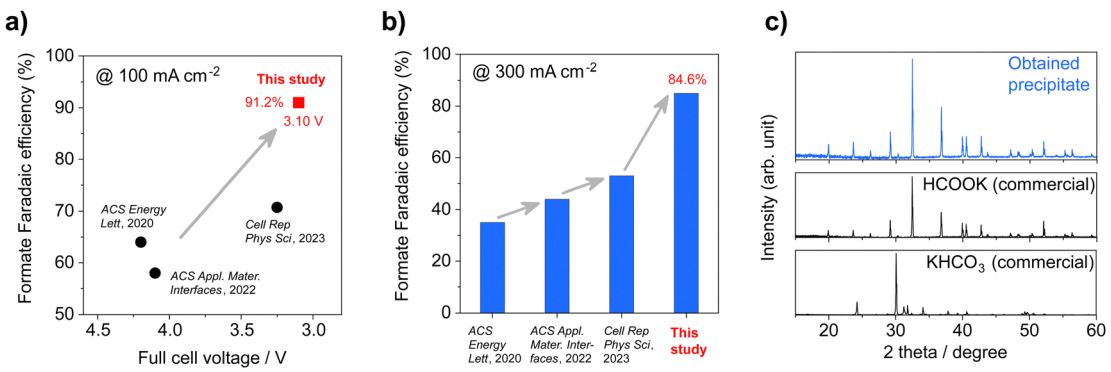

Fig. 6 Comparison of performances with literature on bicarbonate electrolyzers for formate synthesis: (a) formate FE and full cell voltage at 100 mA cm^{-2} and (b) formate FE at 300 mA cm^{-2} (except for *Cell Rep. Phys. Sci.*, 2023 at 200 mA cm^{-2}). (c) Powder XRD patterns of the precipitate obtained by evaporating the catholyte after the bicarbonate electrolyzer reaction (Fig. S10, ESI†) and commercial salts of HCOOK and $KHCO_3$.

of 0.5 M HNO_3 aqueous solution using ultrasonication. A carbon paper (SGL Carbon SIGRACET 39AA) was cut to 4.0 cm (length) × 2.0 cm (width). The carbon paper was immersed 2.0 cm from the bottom edge in the electrodeposition solution, and a constant current of −32 mA (−8 mA cm^{-2}) was applied for 5.0 min to deposit Bi metallic crystallites. The electrode was then washed with deionized water and dried at 80 °C for 10 min. For hydrophobization, 80 μL of 60% PTFE dispersion (Fuel Cell Store Teflon PTFE DISP 30, average particle size ∼0.2 μm) was drop cast on the Bi cathode and heat treated at 250 °C for 30 min.

Characterization was conducted using XRD (Rigaku SmartLab), Raman spectroscopy (Horiba XploRA PLUS), field emission scanning electron microscope (FE-SEM, JEOL JSM-IT800), and contact angle meter (NiCK LSE-B100W).

Bicarbonate-fed electrolysis was performed at ∼25 °C using a two-electrode system. An electrolyzer consisting of end plates, gold-plated current collectors, flow channel plates, and a membrane electrode assembly (MEA) was used. The electrode area is 4 cm^2 (2 cm × 2 cm). Anodes were prepared by spray-coating Pt/CB (Pt 46.4%) or IrO_2 (Ir 74.8%) powders (Tanaka Kikinzoku Kogyo) onto a hydrophobic carbon paper with a microporous layer (SGL Carbon Sigracet 39BC). The catalyst loading was approximately 1 mg cm^{-2}. The ionomer to catalyst weight ratios were 0.5 for Pt/CB and 0.3 for IrO_2, respectively. A Nafion membrane with 5 cm × 5 cm (Chemours N212, thickness 51 μm) was used for PEM. Porous membranes were cut to 2 cm × 2 cm and introduced between the cathode and the PEM as an intermediate layer.

Aqueous $KHCO_3$ solutions were circulated to the cathode at flow rates of 4.0–64 mL min^{-1} using a peristaltic pump. A mass flow controller supplied humidified H_2 at a rate of 50 mL min^{-1} to the Pt/CB anode for HOR. When an IrO_2 anode was used for OER, ultrapure water flowed at the same flow rate as the cathode. A potentiostat (Ivium, Vertex 2A) was used to control and measure voltage and current. The electrochemical reaction test was typically performed by chronopotentiometry at constant current densities. For formate quantification, 1 mL of the electrolyte was collected at a specified time, diluted 1000 times with ultrapure water, and analysed by ion chromatography (Metrohm EcoIC). Proton NMR was also employed for the liquid product analysis (JEOL JMN-ECS300). Gas products were collected using the water displacement method and quantified by gas chromatography. A gas chromatograph equipped with a thermal conductivity detector (Shimadzu GC8A) was used to quantify H_2, and a flame ionization detector with a methanizer (GL Sciences GC3220) was used to quantify CO and CO_2. The faradaic efficiency (FE) of each product was calculated using the formula:

$$\mathrm{FE}\,(\%) = \frac{n \times 2 \times F}{I \times t} \times 100$$

where n is the amount of product [mol], F is the Faraday constant (96 485 C mol^{-1}), I is the current [A], and t is the reaction time [s]. The CO_2 utilization efficiency was calculated from each production rate (v) using the following formula.

$$\text{CO}_2\text{ utilization efficiency}\ (\%) = \frac{v_{\mathrm{Formate}} + v_{\mathrm{CO}}}{v_{\mathrm{Formate}} + v_{\mathrm{CO}} + v_{\mathrm{CO_2}}} \times 100$$

Conclusions

We hypothesized that formate synthesis is more efficient by increasing *in situ* CO_2 generation in bicarbonate-fed electrolyzers. To verify this concept, we installed a hydrophilic cellulose esters membrane between a PEM and a CO_2RR cathode. The protons on PEM transported from the OER anode are neutralized by supplying 3.0 mol L^{-1} $KHCO_3$ at a high flow rate, enhancing the CO_2 generation inside the pores of the mixed cellulose esters membrane. The formate FE reached 91.2% at 100 mA cm^{-2} with a full cell voltage of 3.1 V, and 84.6% even at a high current density of 300 mA cm^{-2}, owing to the enhanced CO_2RR rather than HER on Bi electrocatalyst on the porous cathode. These high FEs and partial current densities (>250 mA cm^{-2}) for formate production demonstrate the innovative design of this reactor in creating a gas–liquid–catalyst triple-phase boundary. The bicarbonate electrolyzer can be operated at low full-cell voltage with long-term stability, providing high CO_2 utilization efficiency. The complete conversion of a carbon-captured solution to the HCOOK solid offers potential for future energy carriers. Thus, combining this bicarbonate electrolyzer with direct formate fuel cells will contribute to green transformation leading to a carbon-neutral society.

Author contributions

K. N., T. O., and K. B. performed the investigation. K. N. and F. A. were responsible for visualisation and writing. T. S. and F. A. were responsible for project administration. All authors contributed to the manuscript's review.

Data availability

The data supporting this article have been included as part of the ESI.†

Conflicts of interest

There are no conflicts to declare.

Acknowledgements

This work was supported by Tokyo Metropolitan Government.

References

1 P. De Luna, C. Hahn, D. Higgins, S. A. Jaffer, T. F. Jaramillo and E. H. Sargent, *Science*, 2019, **364**, eaav3506.
2 N. Han, P. Ding, L. He, Y. Li and Y. Li, *Adv. Energy Mater.*, 2020, **10**, 1–19.
3 X. Yu and P. G. Pickup, *J. Power Sources*, 2008, **182**, 124–132.
4 L. An and R. Chen, *J. Power Sources*, 2016, **320**, 127–139.
5 X. Lu, Y. Wu, X. Yuan and H. Wang, *Angew. Chem., Int. Ed.*, 2019, **58**, 4031–4035.
6 S. Hui, N. Shaigan, V. Neburchilov, L. Zhang, K. Malek, M. Eikerling and P. De Luna, *Nanomaterials*, 2020, **10**, 1–53.

7 Y. Qiao, W. Lai, K. Huang, T. Yu, Q. Wang, L. Gao, Z. Yang, Z. Ma, T. Sun, M. Liu, C. Lian and H. Huang, *ACS Catal.*, 2022, **12**, 2357–2364.
8 K. Liu, W. A. Smith and T. Burdyny, *ACS Energy Lett.*, 2019, **4**, 639–643.
9 J. E. Huang, F. Li, A. Ozden, A. S. Rasouli, F. P. G. de Arquer, S. Liu, S. Zhang, M. Luo, X. Wang, Y. Lum, Y. Xu, K. Bertens, R. K. Miao, C. T. Dinh, D. Sinton and E. H. Sargent, *Science*, 2021, **372**, 1074–1078.
10 J. A. Rabinowitz and M. W. Kanan, *Nat. Commun.*, 2020, **11**, 10–12.
11 E. R. Cofell, U. O. Nwabara, S. S. Bhargava, D. E. Henckel and P. J. A. Kenis, *ACS Appl. Mater. Interfaces*, 2021, **13**, 15132–15142.
12 J. M. Álvarez-Gómez and A. S. Varela, *Energy Fuels*, 2023, **37**, 15283–15308.
13 D. W. Keith, G. Holmes, D. S. Angelo and K. Heidel, *Joule*, 2018, **2**, 1573–1594.
14 R. E. Siegel, S. Pattanayak and L. A. Berben, *ACS Catal.*, 2023, **13**, 766–784.
15 D. J. D. Pimlott, Y. Kim and C. P. Berlinguette, *Acc. Chem. Res.*, 2024, **57**, 1007–1018.
16 G. Lee, A. S. Rasouli, B. H. Lee, J. Zhang, D. H. Won, Y. C. Xiao, J. P. Edwards, M. G. Lee, E. D. Jung, F. Arabyarmohammadi, H. Liu, I. Grigioni, J. Abed, T. Alkayyali, S. Liu, K. Xie, R. K. Miao, S. Park, R. Dorakhan, Y. Zhao, C. P. O'Brien, Z. Chen, D. Sinton and E. Sargent, *Joule*, 2023, **7**, 1277–1288.
17 Y. C. Xiao, C. M. Gabardo, S. Liu, G. Lee, Y. Zhao, C. P. O'Brien, R. K. Miao, Y. Xu, J. P. Edwards, M. Fan, J. E. Huang, J. Li, P. Papangelakis, T. Alkayyali, A. Sedighian Rasouli, J. Zhang, E. H. Sargent and D. Sinton, *EES Catal.*, 2023, **1**, 54–61.
18 Z. Zhang, E. W. Lees, F. Habibzadeh, D. A. Salvatore, S. Ren, G. L. Simpson, D. G. Wheeler, A. Liu and C. P. Berlinguette, *Energy Environ. Sci.*, 2022, **15**, 705–713.
19 T. Li, E. W. Lees, M. Goldman, D. A. Salvatore, D. M. Weekes and C. P. Berlinguette, *Joule*, 2019, **3**, 1487–1497.
20 T. Li, E. W. Lees, Z. Zhang and C. P. Berlinguette, *ACS Energy Lett.*, 2020, **5**, 2624–2630.
21 O. Gutiérrez-Sánchez, B. De Mot, M. Bulut, D. Pant and T. Breugelmans, *ACS Appl. Mater. Interfaces*, 2022, **14**, 30760–30771.
22 Z. Zhang, D. Xi, Z. Ren and J. Li, *Cell Rep. Phys. Sci.*, 2023, **4**, 101662.
23 H. Song, C. A. Fernández, H. Choi, P. W. Huang, J. Oh and M. C. Hatzell, *Energy Environ. Sci.*, 2024, **17**, 3570–3579.
24 C. Delacourt, P. L. Ridgway, J. B. Kerr and J. Newman, *J. Electrochem. Soc.*, 2008, **155**, B42.
25 J. A. Steele and R. A. Lewis, *Opt. Mater. Express*, 2014, **4**, 2133.
26 Y. J. Sa, C. W. Lee, S. Y. Lee, J. Na, U. Lee and Y. J. Hwang, *Chem. Soc. Rev.*, 2020, **49**, 6632–6665.
27 M. F. Liu, C. Zhang, J. Wang, X. Han, W. Hu and Y. Deng, *Chem. – Eur. J.*, 2024, **30**, e202303711.
28 Z. Zhang, E. W. Lees, S. Ren, B. A. W. Mowbray, A. Huang and C. P. Berlinguette, *ACS Cent. Sci.*, 2022, **8**, 749–755.
29 Y. Kim, E. W. Lees and C. P. Berlinguette, *ACS Energy Lett.*, 2022, **7**, 2382–2387.
30 B. De Mot, J. Hereijgers, N. Daems and T. Breugelmans, *Chem. Eng. J.*, 2022, **428**, 131170.
31 M. Ramdin, A. R. T. Morrison, M. De Groen, R. Van Haperen, R. De Kler, L. J. P. Van Den Broeke, J. P. Martin Trusler, W. De Jong and T. J. H. Vlugt, *Ind. Eng. Chem. Res.*, 2019, **58**, 1834–1847.
32 W. Schmittinger and A. Vahidi, *J. Power Sources*, 2008, **180**, 1–14.
33 D. J. D. Pimlott, A. Jewlal, Y. Kim and C. P. Berlinguette, *J. Am. Chem. Soc.*, 2023, **145**, 25933–25937.
34 Y. Chen, A. Vise, W. E. Klein, F. C. Cetinbas, D. J. Myers, W. A. Smith, W. A. Smith, W. A. Smith, T. G. Deutsch and K. C. Neyerlin, *ACS Energy Lett.*, 2020, **5**, 1825–1833.